Inorganic Chemistry
Article

Inorg. Chem. **2010**, *49*, 1865–1871 **1865**
DOI: 10.1021/ic902241n

Unique (3,12)-Connected Porous Lanthanide−Organic Frameworks Based on Ln_4O_4 Clusters: Synthesis, Crystal Structures, Luminescence, and Magnetism

Xia Li,*,† Hao-Ling Sun,*,‡ Xiao-Shuo Wu,† Xiao Qiu,† and Miao Du*,§

†*Department of Chemistry, Capital Normal University, Beijing 100048, People's Republic of China,*
‡*Department of Chemistry, Beijing Normal University, Beijing 100875, People's Republic of China, and*
§*College of Chemistry and Life Science, Tianjin Key Laboratory of Structure and Performance for Functional Molecule, Tianjin Normal University, Tianjin 300387, People's Republic of China*

Received November 13, 2009

Three porous lanthanide−organic frameworks, $[Ln_4(OH)_4(3\text{-SBA})_4(H_2O)_4]\cdot nH_2O$ [Ln = Eu^{III} (**1**), n = 10; Gd^{III} (**2**), n = 10; Tb^{III} (**3**), n = 8; 3-SBA = 3-sulfobenzoate], have been prepared by a hydrothermal synthesis method. They are isomorphous and crystallize in a tetragonal system with space group $P\bar{4}2_1c$. The structure can be considered to be built up by cubanelike $[Ln_4(OH)_4]^{8+}$ secondary building units, which are further connected by 3-SBA to form a 3D coordination framework with 1D pores along the *c* direction for accommodation of novel T8(3) water tapes or zigzag water chains. Furthermore, in these compounds, the $[Ln_4(OH)_4]^{8+}$ units and 3-SBA ligands serve as 12-connected and 3-connected nodes, respectively, resulting in a unique (3,12)-connected framework with the Schläfli symbol of $(4^3)_4(4^{20}.6^{28}.8^{18})$. The luminescent properties of the Eu^{III} (**1**) and Tb^{III} (**3**) complexes have been studied, showing characteristic emissions at room temperature. Variable-temperature magnetic susceptibility studies indicate that the Gd^{III} complex **2** displays weak antiferromagnetic coupling through μ_3-OH^- pathways.

Introduction

In recent years, metal−organic frameworks have been developed rapidly because of their fascinating structures and potential applications as functional materials, in adsorption,[1] ion exchange,[2] chirality,[3] catalysis,[4] luminescence[5] and magnetism.[6] Among them, porous networks[7−11] that allow the reversible passage of molecules through their structures via holes in their surface have attracted particular interest because they provide a good opportunity for the construction of multifunctional materials such as porous magnetic[8a−f] or luminescent materials,[8g] which are in the current forefront of molecular-based materials. A common approach for the construction of porous frameworks is to employ organic

*To whom correspondence should be addressed. E-mail: xiali@mail.cnu.edu.cn (X.L.), haolingsun@bnu.edu.cn (H.-L.S.), dumiao@public.tpt.tj.cn (M.D.).

(1) (a) Park, Y. K.; Choi, S. B.; Kim, H.; Kim, K.; Won, B. H.; Choi, K.; Choi, J. S.; Ahn, W. S.; Won, N.; Kim, S.; Jung, D. H.; Choi, S. H.; Kim, G. H.; Cha, S. S.; Jhon, Y. H.; Yang, J. K.; Kim, J. *Angew. Chem., Int. Ed.* **2007**, *119*, 8378. (b) Ghosh, S. K.; Zhang, J. P.; Kitagawa, S. *Angew. Chem., Int. Ed.* **2007**, *119*, 8111. (c) Han, S. S.; Goddard, W. A. *J. Am. Chem. Soc.* **2007**, *129*, 8422. (d) Hasegawa, S.; Horike, S.; Matsuda, R.; Furukawa, S.; Mochizuki, K.; Kinoshita, Y.; Kitagawa, S. *J. Am. Chem. Soc.* **2007**, *129*, 2607. (e) Dong, Y. B.; Zhang, Q.; Liu, L. L.; Ma, J. P.; Tang, B.; Huang, R. Q. *J. Am. Chem. Soc.* **2007**, *129*, 1514. (f) Hu, S.; He, K. H.; Zeng, M. H.; Zou, H. H.; Jiang, Y. M. *Inorg. Chem.* **2008**, *47*, 5218.

(2) Zhang, J.; Liu, R.; Feng, P. Y.; Bu, X. H. *Angew. Chem., Int. Ed.* **2007**, *119*, 8540.

(3) (a) Bradshaw, D.; Claridge, J. B.; Cussen, E. J.; Prior, T. J.; Rosseinsky, M. J. *Acc. Chem. Res.* **2005**, *38*, 273. (b) Milon, J.; Daniel, M. C.; Kaiba, A.; Guionneau, P.; Brandés, S.; Sutter, J. P. *J. Am. Chem. Soc.* **2007**, *129*, 13872. (c) Xiong, R. G.; You, X. Z.; Abrahams, B. F.; Xue, Z.; Che, C. M. *Angew. Chem., Int. Ed.* **2001**, *40*, 4422. (d) Kesanli, B.; Cui, Y.; Lin, W. *Angew. Chem., Int. Ed.* **2005**, *44*, 72. (e) Li, G.; Yu, W.; Ni, J.; Liu, T.; Liu, Y.; Sheng, E.; Cui, Y. *Angew. Chem., Int. Ed.* **2008**, *47*, 1245. (f) Ma, L.; Abney, C.; Lin, W. *Chem. Soc. Rev.* **2009**, *38*, 1248.

(4) (a) Seo, J. S.; Whang, D.; Lee, H.; Jun, S. I.; Oh, J.; Jeon, Y. J.; Kim, K. *Nature* **2000**, *404*, 983. (b) Han, J. W.; Hill, C. L. *J. Am. Chem. Soc.* **2007**, *129*, 15094. (c) Lee, J.; Farha, O. K.; Roberts, J.; Scheidt, K. A.; Nguyen, S. T.; Hupp, J. T. *Chem. Soc. Rev.* **2009**, *38*, 1450.

(5) (a) Rieter, W. J.; Taylor, K. M. L.; Lin, W. *J. Am. Chem. Soc.* **2007**, *129*, 9852. (b) Bettencourt-Dias, A.; Viswanathan, S.; Rollett, A. *J. Am. Chem. Soc.* **2007**, *129*, 15436. (c) Chen, W. T.; Fukuzumi, S. *Inorg. Chem.* **2009**, *48*, 3800. (d) Lan, A.; Li, K.; Wu, H.; Olson, D. H.; Emge, T. J.; Ki, W.; Hong, M.; Li, J. *Angew. Chem., Int. Ed.* **2009**, *48*, 2334. (e) Allendorf, M. D.; Bauer, C. A.; Bhakta, R. K.; Houka, R. J. T. *Chem. Soc. Rev.* **2009**, *38*, 1330.

(6) (a) Akhtar, M. N.; Zheng, Y. Z.; Lan, Y. H.; Mereacre, V.; Anson, C. E.; Powell, A. K. *Inorg. Chem.* **2009**, *48*, 3502. (b) Wang, X. Y.; Wang, Z. M.; Gao, S. *Chem. Commun.* **2008**, 281. (c) Zeng, M. H.; Wu, M. C.; Liang, H.; Zhou, Y. L.; Chen, X. M.; Ng, S. *Inorg. Chem.* **2007**, *46*, 7241. (d) Kurmoo, M. *Chem. Soc. Rev.* **2009**, *38*, 1353.

(7) (a) Kitagawa, S.; Kitaura, R.; Noro, S. I. *Angew. Chem., Int. Ed.* **2004**, *43*, 2334. (b) Ferey, G. *Chem. Soc. Rev.* **2008**, *37*, 191.

(8) (a) Halder, G. J.; Kepert, C. J.; Moubaraki, B.; Murray, K. S.; Cashion, J. D. *Science* **2002**, *298*, 1762. (b) Wang, Z.; Zhang, B.; Fujiwara, H.; Kobayashi, H.; Kurmoo, M. *Chem. Commun.* **2004**, 416. (c) Kurmoo, M.; Kumagai, H.; Chapman, K. W.; Kepert, C. J. *Chem. Commun.* **2005**, 3012. (d) Kurmoo, M.; Kumagai, H.; Akita-Tanaka, M.; Inoue, K.; Takagi, S. *Inorg. Chem.* **2006**, *45*, 1627. (e) Zhang, X. M.; Hao, Z. M.; Zhang, W. X.; Chen, X. M. *Angew. Chem., Int. Ed.* **2007**, *46*, 3456. (f) Zeng, M. H.; Feng, X. L.; Zhang, W. X.; Chen, X. M. *Dalton Trans.* **2006**, 5294. (g) Zhu, W. H.; Wang, Z. M.; Gao, S. *Inorg. Chem.* **2007**, *46*, 1337.

(9) (a) Belanger, S.; Hupp, J. T.; Stern, C. L.; Slone, R. V.; Watson, D. F.; Carrell, T. G. *J. Am. Chem. Soc.* **1999**, *121*, 557. (b) Rowsell, J. L. C.; Yaghi, O. M. *Microporous Mesoporous Mater.* **2004**, *73*, 3.

Published on Web 01/19/2010

bridging ligands to link metal centers to obtain special structures, such as pillar-layered structures with voids within the solid, in which the pore size can be controlled to some content by changes in the length of the spacer. However, the pore size of these frameworks cannot be as large as we expect because of the fact that when the pore size is large enough, two or more identical frameworks are usually interwoven at the expense of the pore volume, resulting in the occurrence of interpenetration.[9] In order to overcome this obstacle, metal clusters are used as secondary building units (SBUs) for the construction of coordination frameworks with large pore sizes because the bulked metal clusters can increase the critical pore size for interpenetration.[10] As well as the increase of the pore size, the metal clusters can also serve as high-connected nodes, which can produce high-connected frameworks with unique network topology.[10]

Lanthanide−organic frameworks have attracted interest because of their ability to incorporate both photoluminescent and magnetic properties, making them ideal for developing new multifunctional materials.[10d,11,12] However, porous lanthanide−organic frameworks are relatively rare.[11] One possible reason is that the lanthanide ions adopt high coordination numbers and versatile coordination behaviors, which make the coordination spheres of lanthanide cations more difficult to control, in the absence of design strategies for such crystalline solids. Thus, it is significantly more difficult to achieve the target materials with specific properties. Furthermore, the high affinity of lanthanides for oxygen donor atoms makes the oxygen-containing ligands excellent candidates as bridging ligands for the preparation of stable architectures.[11,12] Until now, many lanthanide coordination frameworks with interesting topology and various pore structures including cages and channels have been constructed by using multicarboxylate ligands.[11] However, relatively rare lanthanide coordination frameworks containing other oxygen-containing groups, such as sulfonate, have been reported,[13] in which a few sulfonate-containing porous lanthanide−organic frameworks were documented.[13h,i] In addition, our recent results based on 3-sulfobenzoate (3-SBA) give us a clue on how to rationally construct such porous materials by using this ligand and multinuclear lanthanide clusters.[13b] Herein, we present the hydrothermal synthesis, X-ray crystal structural characterization, and luminescent and magnetic properties of three novel isostructural lanthanide−organic frameworks by using the multidentate ligand 3-SBA. These coordination frameworks with 1D channels are constructed by 12-connected cubanelike $[Ln_4(OH)_4]^{8+}$ units and 3-connected 3-SBA ligands, resulting in unique (3,12)-connected frameworks with the Schläfli symbol of $(4^3)_4(4^{20}.6^{28}.8^{18})$.

Experimental Section

Elemental analyses of carbon, hydrogen, and nitrogen were carried out with an Elementar Vario EL. FTIR spectra of the three compounds were obtained in the range of 4000−400 cm^{-1} on a Nicolet Magna 750 FT/IR spectrometer. The fluorescence spectra and fluorescence decay lifetimes of the solid samples **1** and **3** were recorded on an Edinburgh Analytical Instruments FLS920 spectrometer at room temperature. Variable-temperature magnetic susceptibility measurements of **2** were performed on an MPMS-7 SQUID magnetometer. The experimental susceptibilities were corrected for the diamagnetism of the constituent atoms (Pascal's tables)[14] and the background of the sample holder. Thermogravimetric analyses (TGA) were carried out using a HCT-2 thermal analyzer under air, from room temperature to ca. 1000 °C, with a heating rate of 10 °C/min. Powder X-ray diffraction (PXRD) patterns were collected in the range of $5° < 2\theta < 50°$ at different temperatures on bulk samples with a Bruker AXS D8 ADVANCE diffractometer with Cu Kα radiation in flat-plate geometry. The experimental PXRD patterns match well the calculated ones obtained from the single-crystal structures, confirming the phase purity of the bulk samples.

Synthesis. All of the starting materials were commercially available reagents for analytical grade and were used without further purification. Lanthanide nitrates were produced from lanthanide oxides and nitric acid.

$[Ln_4(OH)_4(3\text{-}SBA)_4(H_2O)_4]\cdot nH_2O$ [Ln = Eu (1), n = 10; Gd (2), n = 10; Tb (3), n = 8]. A mixture of $Ln(NO_3)_3\cdot 6H_2O$ [Ln = Eu (**1**), Gd (**2**), and Tb (**3**)] (0.6 mmol), 3-sulfobenzoic acid (0.6 mmol), 2,2′-bipyridine (0.4 mmol), H_2O (10 mL), and an aqueous solution of NaOH (1.0 mmol) was heated in a 25-mL-capacity stainless steel reactor with a Teflon liner at 150 °C for 3 days under autogenous pressure and then cooled slowly to room temperature. Block crystals of the title complexes suitable for XRD analysis were obtained. Yield: about 44%. Anal. Calcd for $C_{28}H_{48}Eu_4O_{38}S_4$ (**1**): C, 19.45; H, 2.80. Found: C, 19.50; H, 2.86. Selected IR (KBr pellet, ν/cm^{-1}): 3556br, 1596s, 1555vs, 1453s, 1400vs, 1210vs, 1169s, 1107s, 1056s, 769m, 665m, 610s, 575m, 442w. Anal. Calcd for $C_{28}H_{48}Gd_4O_{38}S_4$ (**2**): C, 19.22; H, 2.76. Found: C, 19.65; H, 2.60. Selected IR (KBr pellet, ν/cm^{-1}): 3492br, 1597s, 1556s, 1435s, 1400vs, 1212vs, 1169s, 1107s, 1057s, 769m, 665m, 610s, 575m, 444w. Anal. Calcd for $C_{28}H_{48}Tb_4O_{36}S_4$ (**3**): C, 19.55; H, 2.58. Found: C, 19.68; H, 2.35. Selected IR (KBr pellet, ν/cm^{-1}): 3491br, 1597s, 1556vs, 1435s, 1401vs, 1213vs, 1169s, 1106s, 1075m, 769m, 666m, 611s, 576m, 446w.

(10) (a) Tranchemontagne, D. J.; Mendoza-Cortes, J. L.; O'Keeffe, M.; Yaghi, O. M. *Chem. Soc. Rev.* **2009**, *38*, 1257. (b) Perry, J. J.; Perman, J. A.; Zaworotko, M. J. *Chem. Soc. Rev.* **2009**, *38*, 1400. (c) Yaghi, O. M.; O'Keeffe, M.; Ockwig, N. W.; Chae, H. K.; Eddaoudi, M.; Kim, J. *Nature* **2003**, *423*, 705. (d) Ma, B. Q.; Zhang, D. S.; Gao, S.; Jin, T. Z.; Yan, C. H.; Xu, G. X. *Angew. Chem., Int. Ed.* **2000**, *39*, 3644. (e) Chen, L.; Jiang, F.; Lin, Z.; Zhou, Y.; Yue, C.; Hong, M. C. *J. Am. Chem. Soc.* **2005**, *127*, 8588. (f) Zhang, M. B.; Zhang, J.; Zheng, S. T.; Yang, G. Y. *Angew. Chem., Int. Ed.* **2005**, *44*, 1385. (g) Cairns, A. J.; Perman, J. A.; Wojtas, L.; Kravtsov, V. C.; Alkordi, M. H.; Eddaoudi, M.; Zaworotko, M. J. *J. Am. Chem. Soc.* **2008**, *130*, 1560.

(11) (a) Qiu, Y.; Deng, H.; Yang, S.; Mou, J.; Daiguebonne, C.; Kerbellec, N.; Guillou, O.; Batten, S. R. *Inorg. Chem.* **2009**, *48*, 3976. (b) Black, C. A.; Costa, J.; Fu, W. T.; Massera, C.; Roubeau, O.; Teat, S. J.; Aromi, G.; Gamez, P.; Reedijk, J. *Inorg. Chem.* **2009**, *48*, 1062. (c) Ma, S.; Yuan, D.; Wang, X. S.; Zhou, H. C. *Inorg. Chem.* **2009**, *48*, 2072. (d) Michaelides, A.; Skoulika, S.; Bakalbassis, E. G.; Mrozinski, J. *Cryst. Growth Des.* **2003**, *3*, 487. (e) Chen, X. Y.; Zhao, B.; Shi, W.; Xia, J.; Cheng, P.; Liao, D. Z.; Yan, S. P.; Jiang, Z. H. *Chem. Mater.* **2005**, *17*, 2866. (f) Pan, L.; Woodlock, E. B.; Wang, X. *Inorg. Chem.* **2000**, *39*, 4174. (g) Pan, L.; Adams, K. M.; Hernandez, H. E.; Wang, X.; Zheng, C.; Hattori, Y.; Kaneko, K. *J. Am. Chem. Soc.* **2003**, *125*, 3062.

(12) (a) Huang, W.; Wu, D.; Zhou, P.; Yan, W.; Guo, D.; Duan, C.; Meng, Q. *Cryst. Growth Des.* **2009**, *9*, 1361. (b) Yan, L.; Yue, Q.; Jia, Q. X.; Lemercier, G.; Gao, E. Q. *Cryst. Growth Des.* **2009**, *9*, 2984. (c) Qin, C.; Wang, X. L.; Wang, E. B.; Su, Z. M. *Inorg. Chem.* **2005**, *44*, 7122. (d) Zheng, X. J.; Jin, L. P.; Gao, S. *Inorg. Chem.* **2004**, *43*, 1600. (e) Hill, R. J.; Long, D. L.; Hubberstey, P.; Schroder, M.; Champness, N. R. *J. Solid State Chem.* **2005**, *178*, 2414. (f) Hill, R. J.; Long, D. L.; Champness, N. R.; Hubberstey, P.; Schroder, M. *Acc. Chem. Res.* **2005**, *38*, 337.

(13) (a) Gańdara, F.; Garcíá-Corteś, A.; Cascales, C.; Gómez-Lor, B.; Gutieŕrez-Puebla, E.; Iglesias, M.; Monge, A.; Snejko, N. *Inorg. Chem.* **2007**, *46*, 3475. (b) Li, X.; Wu, X. S.; Zheng, X. J. *Inorg. Chim. Acta* **2009**, *362*, 2537. (c) Liu, Q. Y.; Xu, L. *Eur. J. Inorg. Chem.* **2005**, 3458. (d) Xiong, R. G.; Zhang, J.; Chen, Z. F.; You, X. Z.; Che, C. M.; Fun, H. K. *J. Chem. Soc., Dalton Trans.* **2001**, 780. (e) Wang, Z.; Ströbele, M.; Zhang, K. L.; Meyer, H.-J.; You, X. Z.; Yu, Z. *Inorg. Chem. Commun.* **2002**, *5*, 230. (f) Shimizu, G. K. H.; Vaidhyanathan, R.; Taylor, J. M. *Chem. Soc. Rev.* **2009**, *38*, 1430. (g) Sonnauer, A.; Nalther, C.; Holppe, H. A.; Senker, J.; Stock, N. *Inorg. Chem.* **2007**, *46*, 9968. (h) Dalgarno, S. J.; Atwood, J. L.; Raston, C. L. *Cryst. Growth Des.* **2007**, *7*, 1763. (i) Du, Z. Y.; Xu, H. B.; Mao, J. G. *Inorg. Chem.* **2006**, *45*, 9780.

(14) Boudreaux, E. A.; Mulay, J. N. *Theory and Application of Molecular Diamagnetism*; John Wiley and Sons: New York, 1976.

Table 1. Crystal Data and Structure Refinement for **1**−**3**

	1	**2**	**3**
formula	$C_{28}H_{48}Eu_4O_{38}S_4$	$C_{28}H_{48}Gd_4O_{38}S_4$	$C_{28}H_{44}Tb_4O_{36}S_4$
fw	1728.74	1749.90	1720.55
cryst syst	tetragonal	tetragonal	tetragonal
space group	$P42_1c$	$P42_1c$	$P42_1c$
a, Å	17.2009(2)	17.1743(3)	17.1205(7)
b, Å	17.2009(2)	17.1743(3)	17.1205(7)
c, Å	8.5389(2)	8.5106(2)	8.4672(6)
V, Å^3	2526.41(7)	2510.26(9)	2481.8(2)
Z	2	2	2
D_{calcd}, g/cm^3	2.273	2.315	2.302
μ (Mo Kα), mm^{-1}	5.171	5.491	5.903
cryst size, mm^3	0.40 × 0.40 × 0.20	0.3 × 0.3 × 0.18	0.08 × 0.06 × 0.05
T_{max} and T_{min}	0.356, 0.214	0.4381, 0.2897	0.7568, 0.6496
θ_{min}, θ_{max}, deg	1.67, 27.56	3.36, 27.61	3.38, 27.63
$F(000)$	1672	1680	1648
data collected	19 336	6186	5558
unique data	2914	2679	2866
obsd data [$I > 2\sigma(I)$]	2859	2541	2606
R_{int}	0.0268	0.0195	0.0262
no. of param	197	197	185
R1[a] [$I > 2\sigma(I)$]	0.0152	0.0188	0.0270
wR2[b] [$I > 2\sigma(I)$]	0.0379	0.0395	0.0553
R1[a] [all data]	0.0157	0.0203	0.0317
wR2[b] [all data]	0.0381	0.0400	0.0569
GOF	1.114	1.013	0.995
$\Delta\rho$[c], e/Å^3	+0.453, −0.437	+0.506, −0.363	+0.750, −0.496
Flack parameter	−0.004(10)	−0.013(11)	0.007(16)

[a] $R1 = \sum||F_o|-|F_c||/\sum|F_o|$. [b] $wR2 = [\sum w(F_o^2-F_c^2)^2]/\sum w(F_o^2)^2]^{1/2}$. [c] Maximum and minimum residual electron densities.

Crystallography. Intensity data for crystals of **1**−**3** were collected on a Bruker Smart Apex II CCD diffractometer with graphite-monochromated Mo Kα radiation (0.710 73 Å) at 293 K. The structures were solved by direct methods and refined with the full-matrix least-squares technique based on F^2 using the *SHELXL* program.[15] All non-hydrogen atoms were refined anisotropically. Hydrogen atoms of the water molecules were located from the difference Fourier maps and refined with restraint of the O−H and H···H distances (0.96 and 1.52 Å, respectively). Other hydrogen atoms were placed at the calculated positions. The details of crystallographic data and selected bond parameters for compounds **1**−**3** are listed in Tables 1 and 2, respectively.

Result and Discussion

Description of the Structures. Structure of $[Eu_4(OH)_4(3\text{-SBA})_4(H_2O)_4]\cdot 10(H_2O)$ (1). Single-crystal X-ray determination reveals that complex **1** contains hydroxyl-bridged tetranuclear clusters $[Eu_4(\mu_3\text{-}OH)_4(H_2O)_4]^{8+}$, which are further connected via 3-SBA ligands to result in a 3D coordination framework with 1D channels along the *c* axis. The asymmetric unit of **1** consists of one Eu^{III} ion, one SBA ligand, one μ_3-hydroxyl, one coordination water molecule, and 2.5 lattice water molecules. The coordination environment of Eu^{III} in **1** is depicted in Figure 1. Each Eu^{III} ion is eight-coordinated by two carboxylate oxygen atoms [Eu−O = 2.370(2) and 2.378(2) Å] from two 3-SBA ligands, two sulfonate oxygen atoms [Eu−O = 2.403(2) and 2.404(2) Å] from two 3-SBA ligands, three oxygen atoms [Eu−O = 2.410(2), 2.414(2), and 2.442(2) Å] from μ_3-OH groups, and one water molecule [Eu−O = 2.499(3) Å] (Figure 1). The EuO_8 polyhedron can be described as a distorted square antiprism. All bond lengths around the metal center are comparable to those found in other reported Eu^{III} complexes. Each Eu^{III} and its three nearest Eu^{III} ions are connected together by four μ_3-hydroxyl bridging ligands, forming a cubanelike cluster $[Eu_4(\mu_3\text{-}OH)_4]^{8+}$ with Eu···Eu distances of 3.828 and 4.012 Å, in which four Eu^{III} ions are located at the corners of the tetrahedron. All triangular faces of the tetrahedron are capped by the μ_3-OH^- ligands. Namely, the Eu^{III} ions and triply bridging

(15) (a) Sheldrick, G. M. *SHELXTL*, version 5.1; Bruker Analytical X-ray Instruments Inc.: Madison, WI, **1998**. (b) Sheldrick, G. M. *SHELX-97*, PC Version; University of Göttingen: Göttingen, Germany, **1997**.

Table 2. Selected Bond Lengths (Å) and Angles (deg) for **1**−**3**

		1[a]	
Eu1−O1	2.403(2)	Eu1−O2c	2.404(2)
Eu1−O4b	2.378(2)	Eu1−O5a	2.370(2)
Eu1−O6	2.410(2)	Eu1−O7	2.499(3)
Eu1−O6d	2.414(2)	Eu1−O6e	2.442(2)
Eu1−Eu1d	3.828(1)	Eu1−Eu1e	4.012(1)
Eu1−Eu1f	3.828(1)		
Eu1−O6−Eu1e	111.52(8)	Eu1f−O6−Eu1e	104.02(8)
Eu1−O6−Eu1f	105.00(8)		
		2[b]	
Gd1−O1	2.391(3)	Gd1−O2c	2.390(3)
Gd1−O4b	2.366(3)	Gd1−O5a	2.354(3)
Gd1−O6	2.400(3)	Gd1−O6d	2.408(3)
Gd1−O6e	2.436(3)	Gd1−O7	2.493(3)
Gd1−Gd1f	3.811(1)	Gd1−Gd1d	3.811(1)
Gd1−Gd1e	3.994(1)		
Gd1−O6−Gd1f	104.88(10)	Gd1f−O6−Gd1e	103.76(10)
Gd1−O6−Gd1e	111.37(10)		
		3[c]	
Tb1−O5a	2.344(4)	Tb1−O4b	2.357(4)
Tb1−O2c	2.372(4)	Tb1−O6	2.379(4)
Tb1−O1	2.379(4)	Tb1−O6d	2.387(4)
Tb1−O6e	2.413(4)	Tb1−O7	2.482(5)
Tb1−Tb1f	3.784(1)	Tb1−Tb1d	3.784(1)
Tb1−Tb1e	3.972(1)		
Tb1−O6−Tb1e	111.94(14)	Tb1f−O6−Tb1e	104.08(15)
Tb1−O6−Tb1f	105.14(15)		

[a] Symmetry codes: a, $-y+{}^3/_2, -x+{}^3/_2, z+{}^1/_2$; b, $-x+{}^3/_2, y-{}^1/_2, -z+{}^1/_2$; c, $y, -x+1, -z$; d, $y, -x+1, -z+1$; e, $-x+1, -y+1, z$; f, $-y+1, x, -z+1$. [b] Symmetry codes: a, $-y-3/2, -x-3/2, z-{}^1/_2$; b, $-x-{}^3/_2, y+{}^1/_2, -z-{}^1/_2$; c, $y, -x-1, -z$; d, $y, -x-1, -z-1$; e, $-x-1, -y-1, z$; f, $-y-1, x, -z-1$. [c] Symmetry codes: a, $-y+{}^1/_2, -x+{}^1/_2, z-{}^1/_2$; b, $-x+{}^1/_2, y+{}^1/_2, -z+{}^3/_2$; c, $y, -x+1, -z+2$; d, $y, -x+1, -z+1$; e, $-x+1, -y+1, z$; f, $-y+1, x, -z+1$.

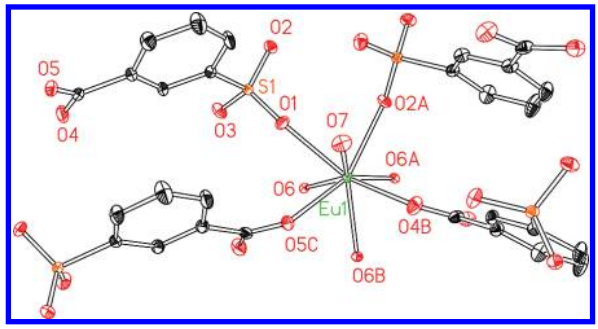

Figure 1. Coordination environment of Eu1 in **1**.

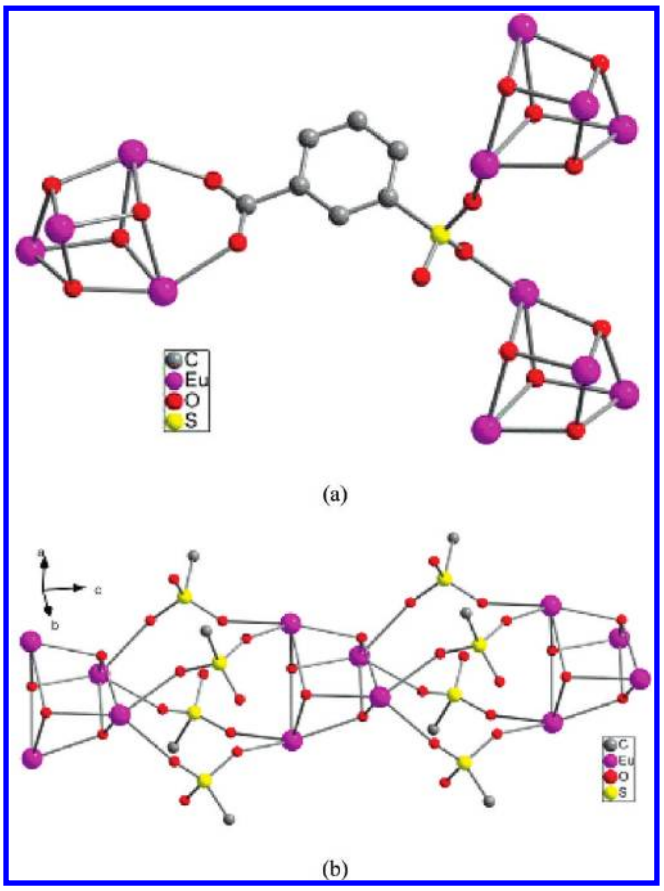

Figure 2. (a) Bridging mode of 3-SBA. (b) 1D chain structure in **1** linked by the Eu_4O_4 tetranuclear unit and μ-SO_3 bridges.

μ_3-hydroxyl groups alternatively occupy the vertexes of the cubane (Figure 2). The cuboidal $[Eu_4(\mu_3\text{-}OH)_4]^{8+}$ core is distorted, with Eu−O−Eu angles of 104.02°, 105.00°, and 111.52°, which are similar to those found in other $[Ln_4(\mu_3\text{-}OH)_4]^{8+}$ clusters.[10d,16]

In **1**, each 3-SBA ligand acts as the three-connected node and links one $[Eu_4(\mu_3\text{-}OH)_4]^{8+}$ SBU through the carboxylate group and the other two through sulfonate. Also, each $[Eu_4(\mu_3\text{-}OH)_4]^{8+}$ SBU is connected to 12 3-SBA ligands to form an infinite framework (Figures 3 and 4). The asymmetric μ_3-bridging mode of 3-SBA results in the overall acentric framework (Figure 2a). Alternatively, the structure of **1** can be viewed as comprising infinite SBUs, in which each sulfonate is linked to two $[Eu_4(\mu_3\text{-}OH)_4]^{8+}$ clusters and each cluster to eight sulfonates, producing a 1D chain along the *c* axis (Figure 2b). The adjacent chains are further connected by the 3-SBA ligands to form a 3D framework. The 3D framework has channels along the [001] direction (Figure 3), which are occupied by lattice water molecules (10 per formula unit). Calculations from the X-ray structure data show that the framework possesses

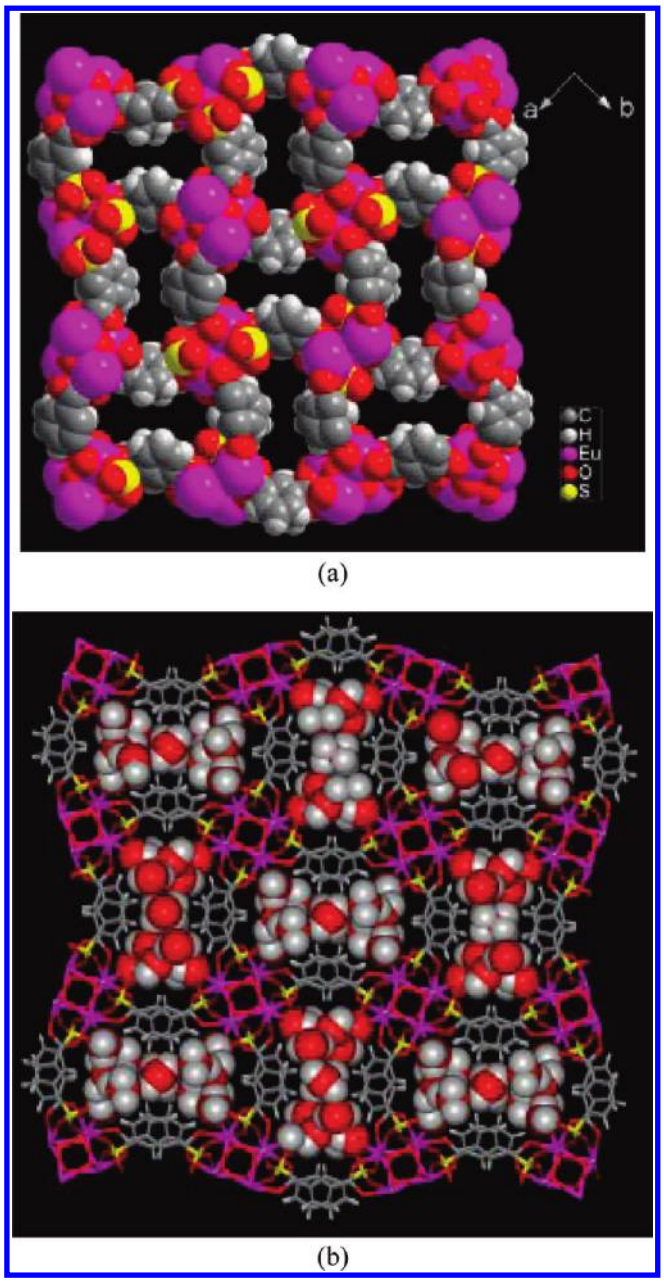

Figure 3. (a) 3D network constructed by the Eu_4O_4 tetranuclear SBUs and 3-SBA bridges with 1D channels along the *c* axis (the coordination and guest water molecules are omitted for clarity). (b) View of the channels in **1**. The coordination and guest water molecules that occupy the channels are shown as space-filling atoms.

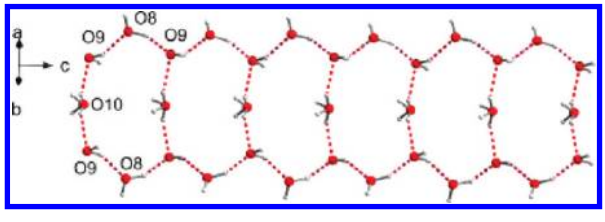

Figure 4. 1D T8(3) water tape constructed by the edge-sharing cyclic octatamers residing in the channels of **1**.

a solvent-accessible volume of ca. 297 $Å^3$, corresponding to 12% of the unit cell. The lattice water molecules are hydrogen-bonded to the channels with O···O distances of 2.628−2.898 Å (Figure 3b and Table 3). To our surprise,

(16) (a) Kajiwara, T.; Katagiri, K.; Hasegawa, M.; Ishii, A.; Ferbinteanu, M.; Takaishi, S.; Ito, T.; Yamashita, M.; Iki, N. *Inorg. Chem.* **2006**, *45*, 4880. (b) Chen, X. M.; Wu, Y. L.; Tong, Y. X.; Sun, Z.; Hendrickson, D. N. *Polyhedron* **1997**, *16*, 4265. (c) Gerasko, O. A.; Mainicheva, E. A.; Naumova, M. I.; Yurjeva, O. P.; Alberola, A.; Vicent, C.; Llusar, R.; Fedin, V. P. *Eur. J. Inorg. Chem.* **2008**, *41*, 416. (d) John, D.; Urland, W. *Z. Anorg. Allg. Chem.* **2007**, *633*, 2587. (e) Rohde, A.; Urland, W. *Dalton Trans.* **2006**, 2974. (f) Wang, R.; Liu, H.; Carducci, M. D.; Jin, T.; Zheng, C.; Zheng, Z. *Inorg. Chem.* **2001**, *40*, 2743. (g) Kong, X. J.; Long, L. S.; Zheng, L. S.; Wang, R.; Zheng, Z. *Inorg. Chem.* **2009**, *48*, 3268.

Table 3. Hydrogen Bond Lengths (Å) and Angles (deg) Associated with Water Molecules

D−H	*d*(D−H)	*d*(H···A)	∠DHA	*d*(D···A)	A
			1		
O7−H3W	0.918	1.838	170.49	2.747	O8 [$-x+{}^{3}/_{2}, y-{}^{1}/_{2}, -z+{}^{1}/_{2}$]
O7−H4W	0.951	2.010	154.63	2.898	O3 [$y, -x+1, -z$]
O8−H5W	1.007	1.678	155.50	2.628	O9 [$x+{}^{1}/_{2}, -y+{}^{3}/_{2}, -z+3/2$]
O8−H6W	0.994	1.879	150.22	2.786	O3
O9−H7W	1.013	1.890	145.25	2.783	O8 [$-y+1, x, -z+1$]
O10−H9W	0.972	2.021	132.06	2.768	O9 [$-x+1, -y+1, z-1$]
			2		
O7−H3W	0.919	1.854	162.20	2.743	O8 [$-x-{}^{3}/_{2}, y+{}^{1}/_{2}, -z-{}^{1}/_{2}$]
O7−H4W	0.943	2.038	150.60	2.897	O3 [$y, -x-1, -z$]
O8−H5W	0.995	1.654	154.17	2.586	O9 [$x-{}^{1}/_{2}, -y-{}^{3}/_{2}, -z-{}^{3}/_{2}$]
O8−H6W	0.992	1.929	143.25	2.788	O3
O9−H7W	1.000	1.933	138.38	2.762	O8 [$-y-1, x, -z-1$]
O10−H9W	0.958	2.175	120.49	2.786	O9 [$-x-1, -y-1, z+1$]
			3		
O7−H3W	0.950	1.816	161.71	2.735	O8 [$-x+{}^{1}/_{2}, y+{}^{1}/_{2}, -z+{}^{3}/_{2}$]
O7−H4W	0.951	2.165	132.57	2.895	O3 [$y, -x+1, -z+2$]
O8−H5W	0.968	1.677	144.92	2.532	O9 [$x-{}^{1}/_{2}, -y+{}^{1}/_{2}, -z+{}^{1}/_{2}$]
O8−H6W	0.965	1.823	170.81	2.780	O3
O9−H7W	0.974	1.755	157.47	2.680	O8 [$-y+1, x, -z+1$]

the lattice water molecules in the channels of the framework show interesting characteristics. Besides forming hydrogen bonds with the oxygen atoms from the sulfonates and the coordinated water of the host framework, the lattice water molecules themselves form cyclic water octamers, and these octamers are further connected into a water tape by sharing the edges (Figure 4). According to Infantes' theory,[17] this water tape is the "T8(3)" type ("T" means "tape", "8" represents the number of water molecules in an individual ring, and "3" means three shared water molecules). Although some examples of octameric water clusters with cubane, open cube, rings, and booklike structures [denoted as "T8(0)"] have been reported,[18] to the best of our knowledge, this is the first example of a T8(3) water tape.

The construction of coordination frameworks by using metal clusters will produce interesting structures with high-connected topology and fascinating properties, which has already been proven.[10] In this paper, the in situ synthesized cubanelike tetranuclear units are further connected by the 3-SBA ligands, resulting in the interesting structure and unique topology. Actually, in this 3D framework, each cubanelike $[Eu_4(\mu_3\text{-}OH)_4]^{8+}$ cluster is connected to 12 organic ligands of 3-SBA, and each ligand is linked to three such tetrameric SBUs, which thus serve as the 12-connected and 3-connected nodes, respectively (Figure 5). As a consequence, the resulting 3D network can be assigned to an unusual two-nodal (3,12)-connected topology (see Figure 5) with the Schläfli symbol of $(4^3)_4(4^{20}.6^{28}.8^{18})$, which, notably, is equivalent to that of the Au_4Ho crystalline lattice[19] and has not been observed in a coordination framework.

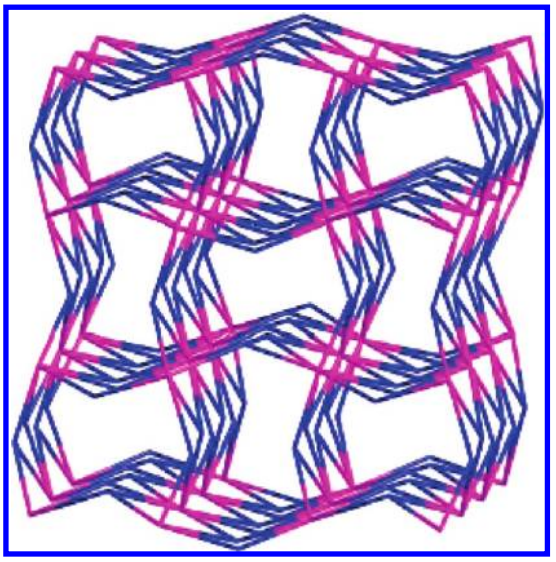

Figure 5. (3,12) network topology of **1**. The 12-connected purple nodes represent the tetranuclear units of Eu_4O_4, while the 3-connected blue ones represent the 3-SBA bridges.

Structures of $[Ln_4(OH)_4(3\text{-}SBA)_4(H_2O)_4]\cdot nH_2O$ [Ln = Gd (2), n = 10; Tb (3), n = 8]. The crystal structures of **2** and **3** are very similar to that of **1**, and it is worth noting that the Ln···Ln separations bridged by μ_3-OH^- are 3.811/3.994 Å for **2** and 3.784/3.972 Å for **3**. The solvent-accessible volumes are ca. 293 and 279 $Å^3$ for **2** and **3**, respectively. The gradual decrease of the Ln···Ln separation and the solvent-accessible volume should arise from the lanthanide contraction effect. Compared with **1**, the solvent-accessible volume in **3** decreases by 18 $Å^3$, which decreases the number of water molecules in the channels and breaks the water tape structure, resulting in 1D zigzag water chains (Figure S1, Supporting Information).

TGA and Temperature-Dependent PXRD. The open channels in the 3D network of $[Ln_4(OH)_4(3\text{-}SBA)_4(H_2O)_4]\cdot nH_2O$ make it possible to generate porous frameworks by

(17) Infantes, L.; Motherwell, S. *CrystEngComm* **2002**, *4*, 454.
(18) (a) Blanton, W. B.; Gordon-Wylie, S. W.; Clark, G. R.; Jordan, K. D.; Wood, J. T.; Geise, U.; Collins, T. J. *J. Am. Chem. Soc.* **1999**, *121*, 3551. (b) Doedens, R. J.; Yphannes, E.; Khan, M. I. *Chem. Commun.* **2002**, 62. (c) Atwood, J. L.; Barbour, L. J.; Ness, T. J.; Raston, C. L.; Raston, P. L. *J. Am. Chem. Soc.* **2001**, *123*, 7192. (d) Ma, B. Q.; Sun, H. L.; Gao, S. *Chem. Commun.* **2005**, 2336.
(19) McMasters, O. D.; Gschneidner, K. A., Jr.; Bruzzone, G.; Palenzona, A. *J. Less-Common Met.* **1971**, *25*, 135.

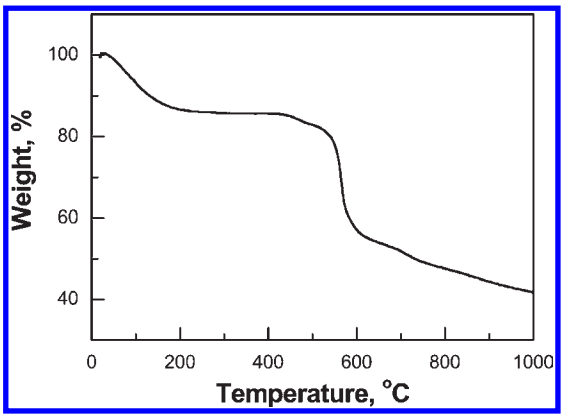

Figure 6. TGA curve of complex **1**.

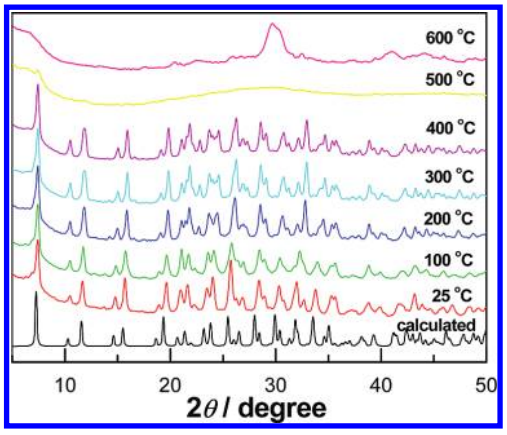

Figure 7. PXRD patterns of **1** at different temperatures.

removing the guest water and/or coordination water molecules. Thermogravimetric analysis (TGA) indicates that **1** loses all water molecules at 217 °C, with a weight loss of 13.6% (calcd 12.8%). Above this temperature to 480 °C, there is no further weight loss, which indicates that the dehydrated framework is thermally stable over a wide range of temperature (Figure 6). Above 480 °C, the TGA curve exhibits a second step of weight loss. The remaining weight of 26.8% indicates that the final product is Eu_2O_3 (calcd 28.8%). The PXRD measurements support the thermal behavior (Figure 7). The measured PXRD pattern closely matches the simulated one obtained from the single-crystal diffraction data. The PXRD patterns at 50, 100, 200, 300, and 400 °C are very similar to that at the room temperature (25 °C). However, the PXRD pattern at 500 °C is clearly different, suggesting a structural change or collapse of the framework. The results of TGA for complexes **2** and **3** are similar to that of complex **1** (Figure S2, Supporting Information). These results indicate the high stability of the frameworks.

Photoluminescent Properties of 1 and 3. The excitation spectrum of **1** monitored at the Eu^{III} $^5D_0 \rightarrow {}^7F_2$ transition (614 nm) consists of a broad band and several narrow bands. The broad band peaking at 286 nm is attributed to the $\pi-\pi^*$ ligand transition, and the narrow bands are assigned to the transitions of Eu^{III} intra-4f^6 ion, from $^7F_0$ to $^5H_4$ (318 nm), $^5G_6$ (362 nm), $^5G_{0-4}$ (377−384 nm), $^5L_6$ (395 nm), and $^5D_3$ (416 nm) (Figure S3, Supporting Information).[20] The emission spectrum of **1** was recorded under the maximum excitation wavelength at 286 nm (Figure 8a). The emission spectrum is composed of the first excited state, $^5D_0$, and the ground septet, ^7F_J (J = 0−4) of Eu^{III}. The transition $^5D_0 \rightarrow {}^7F_0$ is very weak and is situated at 579 nm. The strong transition $^5D_0 \rightarrow {}^7F_1$ splits into three peaks at 587, 594, and 597 nm. The hypersensitive transition $^5D_0 \rightarrow {}^7F_2$ consists of the strongest band at 614 nm with weaker shoulders at 620 and 623 nm, resulting in red fluorescence. The peaks at about 651 and 655 nm correspond to the characteristic $^5D_0 \rightarrow {}^7F_3$ transition. It is also observed that the four splitting peaks of the $^5D_0 \rightarrow {}^7F_4$ transition occur at 691, 697, 700, and 705 nm. The $^5D_0$ lifetime of the Eu^{III} ion was monitored under excitation at 286 nm and the more intense emission at 614 nm ($^5D_0 \rightarrow {}^7F_2$). The emission decay curve reveals a single-exponential behavior, yielding the lifetime value of 0.135 ms ($^5D_0$).

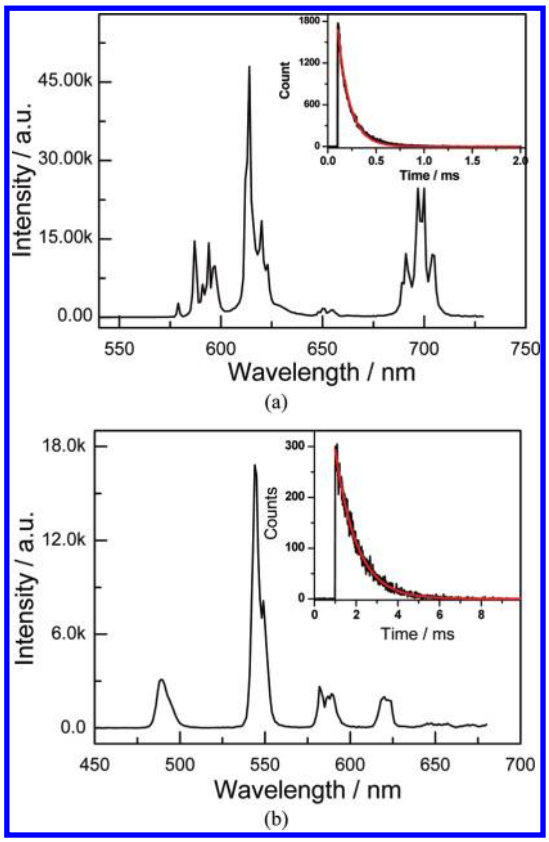

Figure 8. Solid-state emission spectra of **1** (a) and **3** (b).

The excitation spectrum of complex **3** was monitored under the intense $^5D_4 \rightarrow {}^7F_5$ transition (545 nm) of the Tb^{III} ion. A wide absorption band at around 288 nm is attributed to the $\pi-\pi^*$ transition of the ligand, and the narrow excitation bands arise from the intra-4f^8 transition of the Tb^{III} ion at 351 ($^5G_2$), 359 ($^5D_3$), 369 ($^5D_2$), and 377 ($^5D_3$) nm (Figure S3, Supporting Information).[20] The characteristic emission of the Tb^{III} ion from the emitting level ($^5D_4$) to the ground multiplet ($^7F_{6-3}$) is observed upon excitation at 350 nm (Figure 8b). The strongest emission is the hypersensitive transition, $^5D_4 \rightarrow {}^7F_5$, which consists of an intense peak at 545 nm with a shoulder

(20) Girginova, P. I.; Paz, F. A. A.; Soares-Santos, P. C. R.; SáFerreira, R. A.; Carlos, L. D.; Amaral, V. S.; Klinowski, J.; Nogueira, H. I. S.; Trindade, T. *Eur. J. Inorg. Chem.* **2007**, 4238.

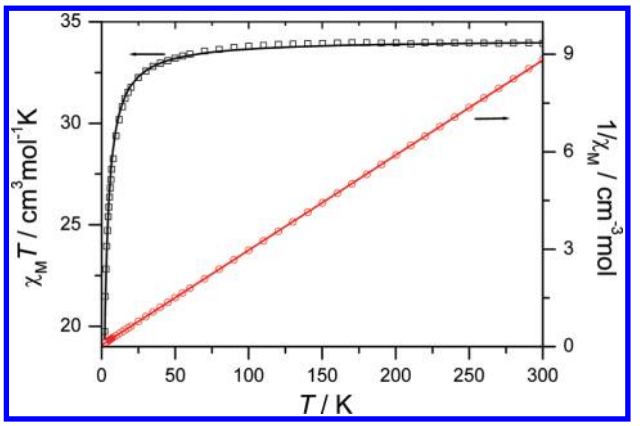

Figure 9. Temperature dependence of $\chi_M T$, and $1/\chi_M$ per Gd_4 unit, for **2**. The full lines represent the best fit to a Curie−Weiss law (see the text).

at 549 nm. The second maximal peak at 489 nm corresponds to the $^5D_4 \rightarrow {}^7F_6$ transition. The $^5D_4 \rightarrow {}^7F_4$ transition consists of weak bands between 582 and 590 nm, while the $^5D_4 \rightarrow {}^7F_3$ transition is the weak peak at 622 nm. The Tb^{III} ion ($^5D_4$) lifetime of compound **3** under excitation of 350 nm and emission of 545 nm is measured to be 1.035 ms.

Magnetic Properties of 2. The variable-temperature magnetic susceptibility $\chi_M T$ per Gd_4 for a collection of crystals of **2** in the temperature range of 2−300 K was measured in a field of 1000 Oe, and the results are shown in Figure 9. The value of $\chi_M T$ at room temperature, 33.94 cm^3 mol^{-1} K, is slightly larger than the spin-only value (31.50 cm^3 mol^{-1} K) expected for four uncoupled $S = {}^7/_2$ spins. The $\chi_M T$ value remains nearly constant at about 50 K and then decreases rapidly to 19.75 cm^3 mol^{-1} K at 2 K, which is similar to that found in other Gd_4O_4 clusters. The magnetic susceptibilities of **2** can be fitted well by the Curie−Weiss law $\chi = C/(T - \theta)$, with $\theta = -1.4$ K and $C = 34.17$ cm^3 mol^{-1} K. The small negative θ value suggests a very weak antiferromagnetic interaction mediated by the μ_3-OH^- pathways. A more detailed analysis shows that the molar magnetic susceptibility can be expressed by the model for cubanelike tetranuclear Gd^{III} compounds provided by John and Urland[16d] with the spin Hamiltonian of $H = -2J(S_{Gd1}S_{Gd2} + S_{Gd1}S_{Gd3} + S_{Gd1}S_{Gd4} + S_{Gd2}S_{Gd3} + S_{Gd2}S_{Gd4} + S_{Gd3}S_{Gd4})$. The best fitting provides $J = -0.031(1)$ cm^{-1}, $g = 2.08(1)$, and $R = 5.4 \times 10^{-5}$ (R is defined as $\sum[(\chi_M)_{obs} - (\chi_M)_{calcd}]^2/\sum[(\chi_M)_{obs}]^2$). The J value is comparable to those found in the reported tetranuclear Gd^{III} complexes.[16d,e]

Conclusions

Three 3D lanthanide−organic frameworks, $[Ln_4(OH)_4(3\text{-}SBA)_4(H_2O)_4]\cdot nH_2O$ [Ln = Eu (**1**), n = 10; Gd (**2**), n = 10; and Tb (**3**), n = 8], have been hydrothermally synthesized by reacting lanthanide nitrates with 3-sulfobenzoic acid. The coordination frameworks show a unique $(4^3)_4(4^{20}.6^{28}.8^{18})$ topology with 12-connected $[Ln_4(\mu_3\text{-}OH)_4]^{8+}$ and 3-connected 3-SBA nodes. Those tetranuclear metal centers are interconnected through 3-SBA ligands to generate 1D channels along the [001] direction, and these channels are occupied by novel T8(3) water tapes or zigzag water chains. Photoluminescence spectra were collected for **1** and **3**, and magnetic susceptibility data for **2** show weak antiferromagnetic coupling between the Gd^{III} ions. Furthermore, the TGA and temperature-dependent PXRD measurements demonstrate their high thermal stability after removal of the guest molecules by heating. Our successful construction of porous lanthanide−organic frameworks by using 3-SBA provides another ligand choice for the design and synthesis of such porous materials, which will be devoted to further finding new porous lanthanide−organic systems and investigating the relationship between their porous and magnetic/fluorescent properties.

Acknowledgment. This work was supported by the National Natural Science Foundation of China (Grant 20801006), the Science and Technology Program, Beijing Municipal Education Commission (Grant KM2009-10028010), and the Natural Science Foundation of Beijing (No. 2103048).

Supporting Information Available: Crystallographic data in CIF format, the water structure found in **3** (Figure S1), TGA data for **2** and **3** (Figure S2), excitation spectra for **1** and **3** (Figure S3), and solid-state emission spectra of **1** [λ_{ex} = 386 nm (a) and 400 nm (b)] at room temperature (Figure S4). This material is available free of charge via the Internet at http://pubs.acs.org. X-ray crystallographic files in CIF format of compounds **1** (CCDC-691664), **2** (CCDC-694433), and **3** (CCDC-682123) can also be obtained free of charge from CCDC, 12 Union Road, Cambridge CB2 1EZ, U.K.; fax +44(0)1223-336033; e-mail deposit@ccdc.cam.ac.uk; url http://www.ccdc.cam.ac.uk/deposit.